First-principles calculation of the pressure dependence of phase equilibria in the Al-Li system

Marcel H. F. Sluiter* and Y. Watanabe
Institute for Materials Research, Tohoku University, 2-1-1 Katahira, Aoba-ku, 980 Sendai, Japan

D. de Fontaine
Department of Materials Science and Mineral Engineering, University of California, Berkeley, California 94720

Y. Kawazoe
Institute for Materials Research, Tohoku University, 2-1-1 Katahira, Aoba-ku, 980 Sendai, Japan

(Received 10 October 1995)

The solid-phase portion of the Al-Li phase diagram has been computed from first principles both at zero pressure and at a hydrostatic compression of 5.4 GPa. Computation of the pressure dependence of the Al-Li phase equilibria answers two questions: (1) how important is the effect of the atomic size difference, and (2) is the stability of the Al_3Li precipitates influenced by high hydrostatic stress. The zero-pressure first-principles phase diagram exhibits excellent qualitative agreement with experimental data. The presence or absence of solid solutions (SS), of stable and metastable intermetallic phases, and their degree of order are computed correctly. Compression is predicted to affect the phase equilibria in Al-Li as follows: (1) the solubility of Li in fcc Al-rich SS is decreased, (2) the solubility of Al in Li is increased. However, the low melting point of Li limits the range of SS, and (3) the metastable Al_3Li Al-rich fcc SS phase equilibrium is unaffected and the stability of the precipitates is unchanged, (4) the ordering tendencies at Li-rich compositions are slightly enhanced. Although high pressure eliminates the difference in atomic volume of the pure constituents, it has almost no effect on the solid-solid phase equilibria in this alloy system. A simple method for verifying the accuracy of the cluster expansion for the configurational internal energy is presented and applied. Moreover, it has been shown that with a convenient choice of the occupation numbers, one can define correlation functions which greatly facilitate the determination of new ground state structures.

I. INTRODUCTION

The stable and metastable phase equilibria in the aluminum-lithium system have been well studied,[1–6] in part because of the technical importance of Al_3Li precipitation hardening in Al-rich Al-Li alloys. *Ab initio* approaches for the study of phase transformations, which do not require any experimental data, are of special interest in the case of the Al-Li system because of the difficulties encountered with experimental determinations of the phase boundaries involving metastable phases. Another advantage of an *ab initio* study of phase equilibria is the predictive, rather than descriptive, nature of such a method and the insight that it provides into the stability of phases.

Here, the phase diagram is computed both at zero hydrostatic pressure, and at 5.4 GPa in order to study the pressure dependence. The computations are facilitated by the fact that the most important phases in the Al-Li system have cubic symmetry, which means that there is a simple relationship between lattice parameter and hydrostatic pressure. Comparing the two phase diagrams, some general effects of pressure are outlined and discussed.

The effect of pressure is of interest both in its own right, and also because it may indicate whether other states of stress affect the phase equilibria. In cases where phase equilibria show a strong response to hydrostatic stress, it is plausible that under actual loading the stability of phases, e.g., phases precipitated during age hardening, can be affected. These issues appear to be especially relevant to the case of Al-Li alloys, where the mechanical properties are enhanced through the precipitation of a metastable phase. Such precipitating phases can be particularly susceptible to stabilization or destabilization as a result of pressure.[7] Moreover, recently, a portion of the high-pressure phase diagram has been determined experimentally,[8] so that some of the computational results can be verified.

Another point of interest is that studying phase equilibria as a function of pressure allows the examination of the size effect in alloy phase stability. Atomic size differences are regarded as a major factor affecting the relative thermodynamic stability of intermetallic phases. The occurrence of certain classes of complex phases such as the A15 and Laves phases is commonly explained in terms of the volumes assigned to the atomic species in the intermetallic compound. Even for the case of ordering and phase segregation on a simple lattice, size effects appear to play a major role, e.g., in the case of ordering in the fcc based Ni-Pt alloys.[9–12] It is therefore of interest to study an alloy where the ratio of the atomic volumes can be easily manipulated. Al-Li alloys are an example of such an alloy; under ambient pressure the volume per atom is about 18% greater in pure Li than it is in pure Al so that a large size mismatch exists. However, the bulk modulus of Li is much smaller than that of Al, so that under hydrostatic compression the atomic volume of Li will decrease much more rapidly than that of Al. At a compression of about 5.4 GPa the atomic volumes in pure Li and pure Al are computed to be about equal. Hence, by studying the Al-Li alloy system as a function of hydrostatic stress one

can examine how the atomic size mismatch affects the phase stability.

The current method can be summarized as follows: The total energies of selected ordered supercells are computed for various values of lattice parameters (i.e., volume per atom) with the linear muffin-tin-orbital–atomic-sphere approximation (LMTO-ASA) method.[13] Minimizing the energy with respect to the volume per atom yields for each ordered structure the equilibrium values of the lattice parameter, the total energy, and the curvature of the total energy with respect to the volume yields the bulk modulus.

Total energies are used to extract chemical interaction energies[14] between the Al and Li species in various crystalline environments as a function of the volume per atom. This method of extracting interactions from total energies has been applied previously to several systems such as Al-Ti,[15] Cd-Mg,[16] Pd-V,[17] Ni-Pt,[10] Ni-Al, and Cu-Pd.[18] The interactions are the coefficients in an Ising-type Hamiltonian, which is solved in an approximate manner, in this case with the cluster variation method (CVM).[19–21] ''Solving this Ising-like Hamiltonian'' means that configurational free energies are computed for each state of order, composition, and temperature. Finally, by combining the configurational free energies of various phases the composition-temperature or the composition-pressure phase diagram is constructed.

Here, we have treated all solid phases that occur in the Al-Li alloy system, including the two complicated line compounds:[4] the Al_4Li_9 phase (space group 12, Pearson designation: $mC26$, $B2/m$, with 26 atoms in the unit cell) (Refs. 22 and 23) and the Al_2Li_3 phase (space group 116, Pearson designation: $hR5$, $R3m$, with 15 atoms in the hexagonal unit cell).[24] The Al_4Li_9 structure can be considered as a fcc or as a bcc superstructure by indexing the a, b, and c lattice vectors as indicated in Table I. However, both the fcc- and bcc-based superstructures have considerable cell external deformation. For the fcc an orthorhombic deformation is needed which can, to a good approximation, be described as a Bain transformation in which in the smallest dimension of the original fcc cube is 27% smaller than the larger two dimensions. The bcc-based representation (see Fig. 1) too, undergoes a Bain-like tetragonalization in which the smaller two dimensions are about 13% smaller than the largest dimension, however, in this case a small shear of about 1.6° in the basal plane is required also. Clearly, the Al_4Li_9 structure is more closely related to the bcc structure. The Al_2Li_3 structure is truly a bcc superstructure in which the $(111)_{bcc}$ planes are exclusively occupied by Li or by Al atoms in a sequence: Li,Al,Li,Li,Al. Three sequences of these stackings (15 planes) give a simple hexagonal cell (see Fig. 1). This structure deviates very little from the underlying bcc structure, there is only a 3.3% expansion along the $\langle 111\rangle$ direction. The rhombohedral unit vectors can be indexed as indicated in Table II. Neither the Al_2Li_3 nor the Al_4Li_9 phase is a known bcc ground state. These phases were included in the phase diagram calculation as line compounds, using experimentally determined atomic positions and under the assumption of perfect configurational order. The latter approximation is suggested by experimental measurements.[22,24] In order to evaluate the effect of the cell internal and cell external relaxations in these two phases, their formation energies have been computed also in the absence of relaxations.

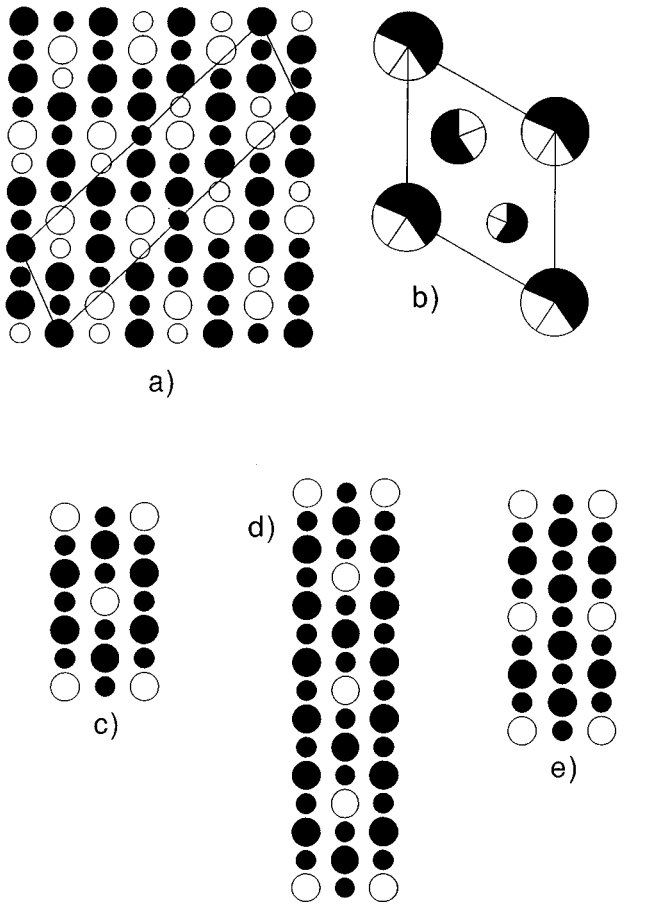

FIG. 1. Kanamori projections of bcc-based ordered structures: (a) Al_4Li_9, (b) Al_2Li_3, (c) $S1$ ($AlLi_5$), (d) $S2$ ($AlLi_6$), (e) $S3$ ($AlLi_7$). All structures are projected onto the (110) plane, except for (b) which is projected onto the (111) plane. Black (white) circles indicate Li (Al) atoms.

In accounting for the hydrostatic pressure it is assumed that the global volume relaxation only is of importance for each superstructure. Of course for noncubic structures, such as the tetragonal $L1_0$ phase, and for structures with cell internal degrees of freedom, such as the Al_2Li_3 phase, this is an approximation. However, the stable and metastable phases of interest in this alloy system have cubic symmetry (fcc, $L1_2$,$B32$), so that this approximation is not likely to be of significance. Moreover, in the Al-rich alloys which are of particular interest, Al and Li have the same partial molar volumes which indicates that relaxations are very small. For example, when the c/a ratio of the tetragonal Al_3Li DO_{22} phase is computed, a value of 1.974 is found which differs insignificantly from the ideal ratio of 2. The c/a relaxation in this phase decreases the total energy by a paltry

TABLE I. Crystallographic relationships between $mC26$ and bcc and fcc.

Lattice vector	$\langle hkl\rangle_{bcc}$	$\langle hkl\rangle_{fcc}$
a	$\langle 4,3,3\rangle$	$\langle 4,3,0\rangle$
b	$\langle -1.5,0.5,0.5\rangle$	$\langle -1.5,0.5,0\rangle$
c	$\langle 0,-1,1\rangle$	$\langle 0,0,1\rangle$

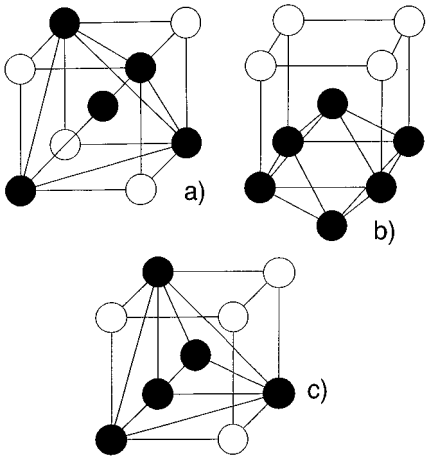

FIG. 2. TOP maximal clusters: (a) centered tetrahedron, (b) octahedron, and (c) pentuplet.

0.0125 mRyd/atom. Hence, the approximation of ignoring deviations from the exact fcc (bcc) lattice positions (volume relaxation is treated only) is well justified in Al-rich alloys which are the main practical interest.

In the current method configurational and static displacement effects are considered only. The effect of phonons is neglected. This neglect should not generally be valid and below we will discuss how vibrational effects might affect our findings.

II. GENERAL METHOD

Total energies of a large number of fcc and bcc superstructures were computed with the LMTO-ASA method.[13] Equal sphere radii were selected for Al and Li, the ''combined corrections'' to the ASA were included, and the von Barth–Hedin parametrization of the exchange correlation potential was used. Care was taken to compute all superstructures with the same k-point grid, which included 1000 points in the first Brillouin zone for the fcc- and bcc-based crystal structures. Formation energies $\Delta E_{\rm form}$ were extracted from the total energies $E_{\rm tot}$ by subtracting the concentration-weighted average of the total energies of the pure elements in the fcc state, according to

$$\Delta E^{\alpha}_{\rm form}(V)=E^{\alpha}_{\rm tot}(V)-c^{\alpha}_{\rm Li}E^{\rm Li\text{-}fcc}_{\rm tot}(V_0)-(1-c^{\alpha}_{\rm Li})E^{\rm Al\text{-}fcc}_{\rm tot}(V_0), \tag{1}$$

where the superscript α refers to a particular superstructure, $c^{\alpha}_{\rm Li}$ is the concentration of the Li species in the α phase, V is the volume per atom, and V_0 refers to the equilibrium value of V. Selecting fcc Li as the standard state for the formation energy is justified on the grounds that Li has the close packed $9R$ structure[25] as ground state which is distinguished from the fcc in the stacking sequence of the dense packed planes only. Hence, the energy difference between the fcc and $9R$ phases should be very small. At constant, nonzero pressure, enthalpies H, rather than energies need to be considered. Enthalpies of formation $\Delta H_{\rm form}$ can be computed with

$$\Delta H^{\alpha}_{\rm form}(P)=H^{\alpha}(P)-c^{\alpha}_{\rm Al}H^{\rm Al\text{-}fcc}(P)-(1-c^{\alpha}_{\rm Al})H^{\rm Li\text{-}fcc}(P), \tag{2}$$

where P is the hydrostatic pressure, and the enthalpy itself is given by

$$H^{\alpha}(P)=E^{\alpha}_{\rm tot}[V(P)]+PV(P). \tag{3}$$

The volume V is found by solving $P=-\partial E_{\rm tot}/\partial V$. At finite temperature one solves $P=-\partial F/\partial V$ to find V, where F is the Helmholtz free energy of formation ($F=E_{\rm form}-TS$).

The total energies are used to obtain effective cluster interactions (ECI) by means of a Connolly-Williams procedure.[26] The ECI J_i for a cluster i are calculated with

$$\sum_{\alpha} w^{\alpha}\left(\Delta E^{\alpha}_{\rm form}(V)-\sum_{i=1}^{n}J_i(V)\xi^{\alpha}_i\right)^2=\text{minimal}, \tag{4}$$

where ξ is the cluster correlation function as defined in Eq. (10) in Ref. 14, and w represents the weights assigned to each structure. In order to make it easier to determine ground states, as will be mentioned below, the occupation numbers for the $B(A)$ atomic species were not selected as $-1(1)$, but rather as $0(1)$. This means that the correlation functions refer to the frequency of the particular cluster configuration of pure A occupancy. The weights are determined according to

$$w^{\alpha}=\frac{1}{1+\omega(d_{\alpha}/\langle d\rangle)^2}, \tag{5}$$

where d_{α} represents the energy difference of a structure α to the convex hull formed by the ground state ordered structures, and $\langle d\rangle$ is that energy difference averaged for all structures. Of course, d_{α} takes the value zero if α is a ground state. ω is a factor which is assigned the smallest positive value which insures that the total energies of all structures are in the correct order, as in the spirit of Ref. 27. In the actual calculations ω was given the value 2 (0) for the fcc (bcc) lattice.

The idea of weighting each structure is as follows: If a structure is very close, or right on the convex hull, it repre-

TABLE II. Crystallographic relationship between $hR5$ and bcc.

Lattice vector	$\langle hkl\rangle_{\rm bcc}$
a	$\langle 1,1,0\rangle$
b	$\langle 1,0,1\rangle$
c	$\langle -2.5,2.5,2.5\rangle$

TABLE III. Number of correlation functions (N_c) and probabilities (N_p) with TOP maximum clusters.

Structure	N_c	N_p
BCC	20	87
$B2$	38	169
$B32$	53	284
$B11$	88	539
DO_3	62	305
$C11_b$	75	426
$S1$	211	1446
$S2$	931	6612
$S3$	177	1068

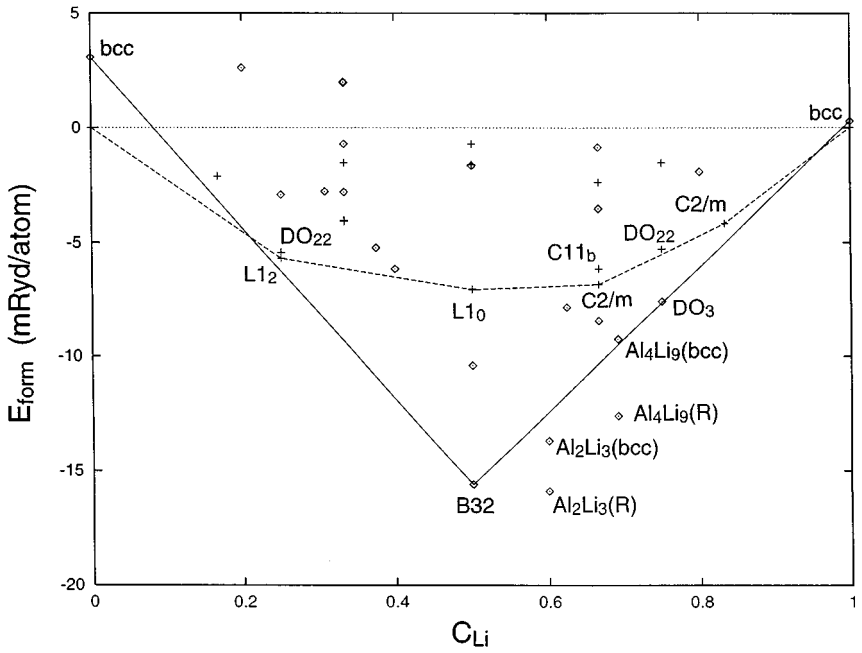

FIG. 3. Formation energies from LMTO-ASA calculations as defined with Eq. (1). Superstructures of the bcc (fcc) lattice are indicated with $\diamond$ $(+)$. The convex hull pertaining to bcc (fcc) ground states is marked with a solid (dotted) line. The Al_2Li_3 and Al_4Li_9 phases are shown both without cell external relaxations as bcc superstructures (bcc) and with cell external relaxations (R).

sents an atomic configuration that occurs with high probability in the actual alloy, and hence it is important that this energy be described accurately. Some other structure that is far above the convex hull represents a configuration that is not very likely to occur in the actual alloy, and thus does not need to be described quite as accurately. Equation (4) was solved using a singular value decomposition procedure. The advantage of this method over the usual Connolly-Williams procedure is that in one calculation not only the values of the ECI are determined but, that in an underdetermined system one also finds at the same time the set of clusters $\{i\}$ which best describe the energetics of the alloy. We have checked that the cluster expansion thus obtained correctly orders the relative stabilities of all phases.[27] An additional benefit of weighting the lowest energy states more heavily in the Connolly-Williams method is that a much more rapid convergence of the cluster expansion is obtained. This has been noticed in particular in ionic systems.[28]

Finally, the energy of any superstructure can be computed with

$$\Delta E^{\alpha}_{\mathrm{form}}(V)=\sum_i \xi^{\alpha}_i J_i(V). \tag{6}$$

The convergence of the cluster expansion of the formation energy has been checked with the following procedure: A set of n ordered structures is selected. Using the ''exact'' (read LMTO-ASA) formation energies of $n-1$ ordered structures, the ECI are computed according to Eq. 4. The ECI are then inserted in Eq. (6) to compute the formation energy of the structure nr n, which has not been included in the calculation of the ECI, and the difference between the ''exact'' value and the ECI predicted value for the formation energy is computed; this difference is referred to as the ''error of the predicted formation energy.'' This procedure is repeated so that each structure is excluded once, such that for each structure the error of the predicted formation energy is calculated. When the error averaged for all structures is greater than some tolerance, the expansion is considered to be unconverged and a LMTO-ASA calculation is carried out for a new structure. If this structure has a composition c_{Li} different from 0.5, both composition c_{Li} and $1-c_{\mathrm{Li}}$ are considered. This procedure was repeated until the average error was less than 1.5 (2.0) mRyd/atom corresponding to a relative error in the formation energy of about 20% (11%) on the fcc (bcc) lattice.

The procedure was started with the set of ground states stabilized by the first (first and second) nearest neighbor (NN) effective pair interactions (EPI) on the fcc (bcc) lattice. This set was expanded with other ground states stabilized by more distant EPI, and also with some simple structures based on alternating occupancies on low index crystallographic planes. For the fcc lattice, the following set of 14 structures was used to extract the ECI: fcc, $L1_0$, $L1_2$, $K40$, DO_{22}, $C2/m$ AB_5 and A_2B_4,[29] and $C11_b$ ($MoPt_2$ prototype). $K40$ refers to structure nr 40 in the fcc ground state analysis by Kanamori and Kakehashi.[42] On the bcc lattice a set of 19 structures was used to compute the ECI: bcc, $B2$, $B32$, DO_3, $C11_b$ ($MoPt_2$ prototype), $B11$, $F9$, $F10$, $F13$, $F17$, unrelaxed Al_4Li_9 and Al_9Li_4, where the structures with prefix ''F'' refer to ground states discovered by Finel.[30] The energies of formation for structures in both sets were reproduced to within a fraction of a mRyd/atom by the fcc and bcc cluster expansions, Eq. (6). The fcc ECI were used to compute the formation enthalpies of all fcc ground state structures stabilized by first and second NN pair interactions.[31,32] The bcc ECI were used to compute the formation enthalpies of all known bcc ground state structures[30] as well as the ''interloper'' phases (i.e., those which cannot be considered as simple superstructures of the fcc and bcc lattices) as mapped onto the bcc crystal structure as described above. CVM calculations on the bcc lattice indicated that at zero pressure an unknown ordered phase should exist between the Li-bcc and the AlLi $B32$ phases. Below, we will indicate how it was determined that such a phase should exist, and how its structure was found.

The phase equilibria at nonzero temperature were determined with the Gibbs free energy

TABLE IV. Total energies at 0 GPa and 5.4 GPa.

Structure	c_{Li} (a/0)	E_{form} (mRyd/atom)	a (Å)	B (GPa)	Structure	c_{Li} (a/0)	E_{form} (mRyd/atom)	a (Å)
fcc	0.0	0	3.999	84.4	fcc	0	0.000	3.913
$C2/m$	0.167	-2.126	4.008	71.0	$C2/m$	0.167	-2.428	3.904
$L1_2$	0.25	-5.676	3.985	70.0	$L1_2$	0.25	-6.704	3.910
DO_{22}	0.25	-5.420	3.995	65.3	DO_{22}	0.25	-6.346	3.901
$C11_b$	0.333	-4.018	4.000	58.8	$C2/m$	0.333	-5.205	3.898
$C2/m$	0.333	-4.070	4.005	58.3	$C11_b$	0.333	-5.265	3.896
$Z3$	0.333	-1.531	4.053	56.6	$Z3$	0.333	-1.830	3.943
$L1_0$	0.5	-7.068	3.979	46.2	$K40$	0.5	-9.969	3.844
$K40$	0.5	-7.048	3.967	45.7	$L1_0$	0.5	-9.312	3.861
$L1_1$	0.5	-1.617	4.021	42.9	$L1_1$	0.5	-3.305	3.884
$Z2$	0.5	-0.721	4.075	46.3	$Z2$	0.5	-0.033	3.957
$C11_b$	0.667	-6.135	4.002	34.1	$C11_b$	0.667	-9.185	3.844
$C2/m$	0.667	-6.832	3.997	34.6	C2/m	0.667	-9.950	3.842
$Z3$	0.667	-2.384	4.075	35.2	$Z3$	0.667	-3.935	3.903
$L1_2$	0.75	-1.534	4.046	26.8	DO_{22}	0.75	-8.346	3.843
DO_{22}	0.75	-5.257	4.023	28.6	$L1_2$	0.75	-4.168	3.852
$C2/m$	0.833	-4.168	4.084	24.6	$C2/m$	0.833	-6.284	3.871
fcc	1.0	0	4.235	14.7	fcc	1	0.000	3.911
bcc	0.0	3.068	3.194	76.1	bcc	0	3.825	3.123
$F17$	0.2	2.616	3.203	61.4	$F17$	0.2	2.731	3.117
DO_3	0.25	-2.897	3.175	58.9	DO_3	0.25	-4.064	3.091
$C11_b$	0.333	2.009	3.199	51.1	$C11_b$	0.3333	-.195	3.104
$F10$	0.333	-2.785	3.180	56.3	$F10$	0.3333	-4.053	3.092
$F13$	0.333	-0.745	3.219	55.1	$F13$	0.3333	-0.370	3.127
$F9$	0.375	-5.251	3.147	54.1	$F9$	0.375	-7.519	3.065
$B2$	0.5	-10.388	3.099	47.9	$B2$	0.5	-14.324	2.999
$B32$	0.5	-15.636	3.140	51.4	$B32$	0.5	-18.637	3.053
$B11$	0.5	-1.693	3.225	44.3	$B11$	0.5	0.165	3.119
$F9$	0.625	-7.873	3.133	37.6	$F9$	0.625	-12.275	3.010
$C11_b$	0.667	-3.528	3.189	33.3	$C11_b$	0.6667	-7.910	3.061
$F10$	0.667	-8.424	3.171	35.7	$F10$	0.6667	-11.828	3.043
$F13$	0.667	-0.877	3.239	34.0	$F13$	0.6667	-1.525	3.112
DO_3	0.75	-7.581	3.177	29.0	DO_3	0.75	-11.489	3.020
$F17$	0.8	-1.905	3.257	25.9	$F17$	0.8	-3.568	3.085
bcc	1.0	0.283	3.367	15.2	bcc	1	0.473	3.110
Al_3Li_2 (bcc)	0.4	-6.131	3.186	53.1				
Al_2Li_3 (bcc)	0.6	-13.644	3.152	43.4				
Al_2Li_3 (relaxed)	0.6	-15.877	-	-				
Al_9Li_4 (bcc)	0.308	-2.773	3.192	60.2				
Al_4Li_9 (bcc)	0.692	-9.250	3.192	35.0				
Al_4Li_9 (relaxed)	0.692	-12.591	-	-				

$$G^{\alpha}=H^{\alpha}-TS^{\alpha}, \tag{7}$$

where T and S are the temperature and entropy, respectively.

The tetrahedron approximation of the CVM was found to be insufficient to accurately represent the states of order and the associated enthalpies of formation. Instead, the tetrahedron-octahedron maximal clusters[29] were used for the fcc and its superstructures, and the centered tetrahedron-octahedron-pentuplet (TOP) maximal clusters were used for

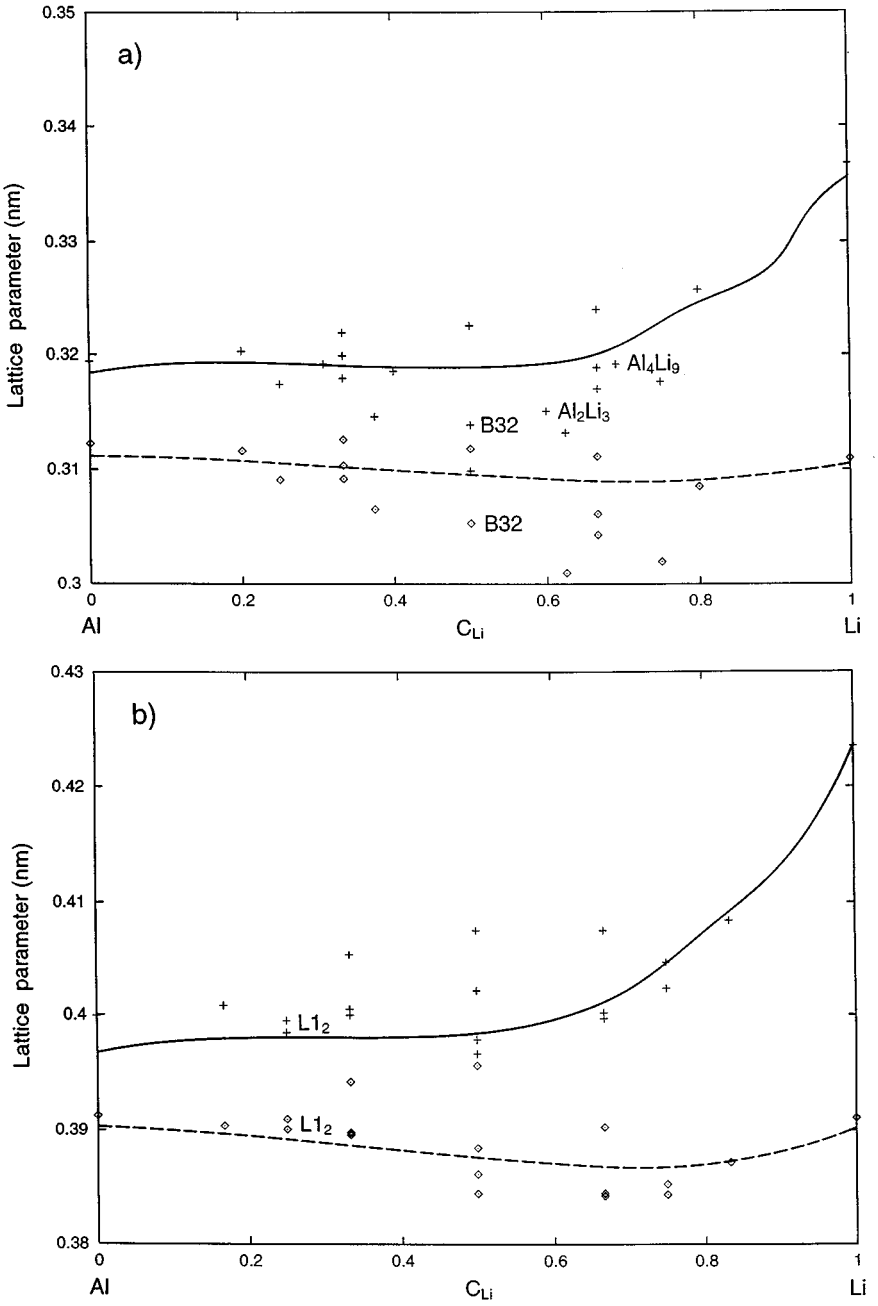

FIG. 4. Variation of the lattice parameter (in nm) with composition and pressure, (a) bcc, (b) fcc. The lattice parameter of the random solid solution is indicated with the continuous line, 0 GPa (solid), 5.4 GPa (dashed); ordered superstructures are marked with symbols, 0 GPa (+), 5.4 GPa ($\diamond$).

the bcc and its superstructures. The TOP maximal clusters, see Fig. 2, were chosen according to the maximal cluster selection rule proposed by Vul and de Fontaine.[33] To the best of the authors' knowledge, the TOP maximal clusters have not been used before. The TOP approximation can treat correlations up to and including the third NN and the number of correlation functions and the number of probabilities that contribute to the CVM expression for the entropy is still rather small, making phase diagram calculations both feasible and accurate (see Table III).

The CVM equation were solved with the Newton Raphson technique as described previously.[14] However, here it is not assumed that the total energy can be expanded as a parabola in terms of the volume per atom; instead a Birch-Murnaghan interpolation to the LMTO-ASA total energies was performed.

III. RESULTS

A. Phase stability at zero temperature

The results from the electronic total energy calculations are summarized in Table IV. At zero pressure, we confirm previous results:[14] ordering is predicted on both the fcc and bcc lattices with as intermetallic ground states, $B32$ AlLi on the bcc lattice and $L1_0$ AlLi and $L1_2$ Al_3Li on the fcc lattice. However, here we considered also ground states which are stabilized by second and more distant neighbor EPI, as well as a few other structures. Consequently some structures were found to break the convex hull of the lattice ground states reported previously.[14] On the fcc lattice the $C2/m$ $AlLi_5$ and $C2/m$ Al_2Li_4 (Ref. 29) were found to be marginally more stable than the two phase mixtures of fcc Li and $L1_0$ AlLi, see Fig. 3. On the bcc lattice no new ground states

were found. In fact, here we find one ground state less than in Ref. 14. The full-potential linearized augmented-plane-wave (FLAPW) method used in that work predicts that the $AlLi_3$ DO_3 phase was marginally stable. In this study, using the LMTO-ASA method, the DO_3 is just not quite stable with respect to a two-phase mixture of bcc Li and AlLi $B32$. The ordered ground states on the fcc lattice at Li-rich compositions appear to contradict the predicted phase segregation tendencies reported in an earlier work.[14] But of course, the ''new'' ground states are all stabilized by ECI beyond the NN shell which were not considered previously. Hence, the previously predicted phase segregation tendency[14] is an artifact caused by limiting the interaction range to the NN shell. Here, the Al_4Li_9 and Al_2Li_3 phases have been included also. The Al_2Li_3 is almost perfectly bcc, and hence its formation energy too can be computed with Eq. (6). In that case, this phase is found to break the convex hull. The bcc form of the Al_4Li_9 phase can be included too, but without the cell external relaxation it is not stable with respect to bcc Li and AlLi $B32$. When the Al_4Li_9 phase is computed with the experimentally measured atomic positions, it is found to be stable with respect to all known bcc superstructures[30] and the Al_2Li_3 structure. As can be expected from the large cell external relaxation, the formation energy of the bcc modification of the Al_4Li_9 phase is much less negative than that of the relaxed structure (with the experimental atomic positions). The Al_2Li_3 structure also is stabilized noticeably by cell external relaxation, see Table IV and Fig. 3. Formation energies of these phases can be compared with those obtained from phase diagram assessments, see Table V. Clearly, the computed formation energies are well within the spread of those obtained from fitting to experimental data. The formation energy of the Al_4Li_9 phase reported in Ref. 4 appears incongruous, and is inconsistent with the phase diagram assessment.

The structural energy differences between fcc and bcc crystal structures for the pure elements also mirror the earlier results[14] where they have been discussed in detail. We find somewhat smaller structural energy differences with the LMTO-ASA than were found previously with an FLAPW calculation: for Al (Li) we find 3.1 (0.3) mRyd/atom as compared to 4.6 (0.5) mRyd reported in previously.[14] Our result for Li is in excellent agreement with another, very careful FLAPW calculation[34] of the Li fcc-bcc structural energy difference of 0.2 mRyd/atom, which is much closer to the LMTO-ASA result in our calculations. The spread in the FLAPW results[14,34] for Li gives an indication of the accuracy of these *ab initio* total energy calculations. Considering that the FLAPW does not assume a spherical potential, we believe that those structural energy differences[34,14] are the most accurate. It should be mentioned that the actual ground state of Li appears to be $9R$,[25] a dense packed hexagonal structure which is related to the fcc structure by a slight variation in the stacking of the close-packed $(111)_{fcc}$ planes. The bulk moduli compare favorably with those computed previously[14,34] and with those measured, see Table VI. In other aspects, such as the particular deviation of the lattice parameter from Vegard's rule (see Fig. 4), and the linear dependence of the bulk modulus on the composition (see Fig. 5) the previous results are confirmed. The bulk modulus of the fcc Al-rich solid solution (SS) decreases by 0.57 GPa for every atomic percent Li added, which is close to the observed values of 0.50 GPa (Ref. 35) and 0.58 GPa,[36] and those found in other calculations: 0.48 GPa,[14] and 0.53 GPa.[34]

TABLE V. Energies of formation at $T=0$ K in mRyd/atom from electronic structure calculations, and from phase diagram assessment (assess) of experimental data.

Structure	Method	Reference	Energy of formation
$B32$	Assess	Ref. 1	-18.0
	Assess	Ref. 4	-11.9
	LMTO-ASA	(this work)	-15.6
	FLAPW	Ref. 14	-16.4
Al_2Li_3	Assess	Ref. 1	-24.1
	Assess	Ref. 4	-11.8
	LMTO-ASA	(this work)	-15.9
	FLAPW	Ref. 60	-14.2
Al_4Li_9	Assess	Ref. 1	-20.7
	Assess	Ref. 4	-16.9
	LMTO-ASA	(this work)	-12.6
	FLAPW	Ref. 60	-11.2
Al_3Li $L1_2$	LMTO-ASA	(this work)	-5.7
	FLAPW	Ref. 14	-8.3
	ASW	Ref. 59	-9.0

A particularly noteworthy feature is the strong variation of the lattice parameter with the state of order: on the bcc lattice the $B11$ configuration has a lattice parameter that is 4% larger than that of the $B2$ state of order. On the fcc lattice the local atomic order also produces large variations in the lattice parameter. When the equilibrium lattice parameter is strongly dependent on the state of order, methods based on a perturbation of the configurationally random alloy, such as the KKR-CPA-GPM method,[37,38] require special care. Typically, in a perturbation approach energies of all states of order are derived from the properties of the random alloy at its equilibrium lattice parameter. When a particular state of order occurs at a lattice parameter far removed from that of the random state, a significant error may be introduced in the energy.

As was reported previously,[14] the technologically important Al-fcc and Al_3Li $L1_2$ phases are computed to have nearly identical lattice parameters, in agreement with the experimental observation that the $L1_2$ phase precipitates as an almost perfectly coherent phase with no lattice mismatch with the Al-rich matrix. At a hydrostatic pressure of 5.4 GPa the lattice mismatch remains very small, and even appears to be getting less. Hence, it is expected that the morphology of the Al_3Li precipitates in Al-rich fcc matrix is unaffected by pressure. Of course, comparing the lattice parameter of stoichiometric $L1_2$ with that of pure fcc Al is not quite correct because in the actual alloy the compositions of the $L1_2$ and fcc matrix are not stoichiometric or pure. Below, when the CVM calculations are discussed, we will return to this point.

One of the parameters which characterizes the strengthening of alloys by ordered precipitates is the specific antiphase boundary (APB) energy. In the case of Al_3Li $L1_2$ precipitation in Al-Li alloys the (111) APB energy determines the strengthening. Measurements on large precipitates[39] formed at elevated temperature indicate a value of about 165

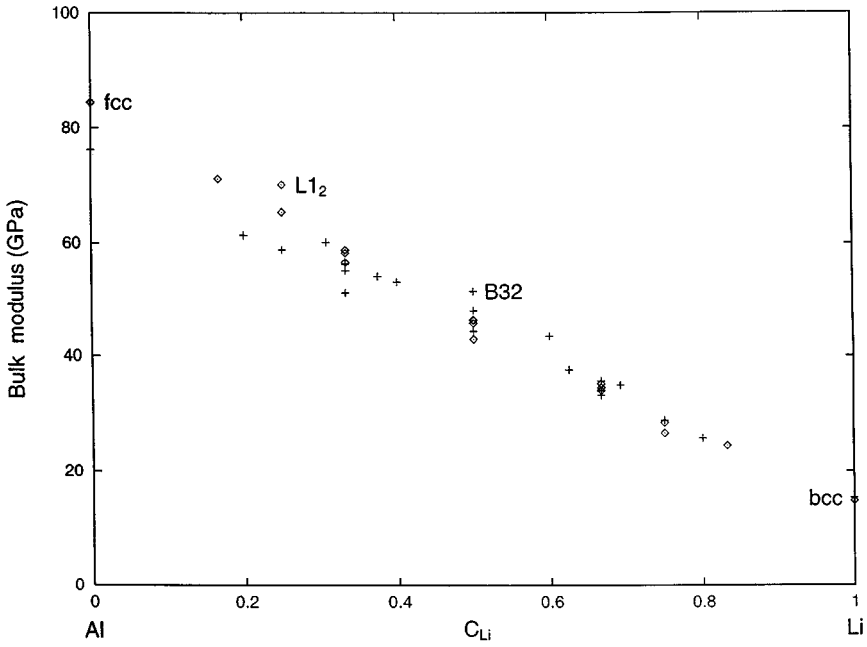

FIG. 5. Bulk modulus (in GPa) as a function of composition. bcc- (fcc-) based structures are indicated with + ($\diamond$).

mJ/m^2. In the smaller precipitates that are formed at room temperature a lower value of about 126 mJ/m^2 is measured.[40] In previous phase diagram fitting work rather lower values were found: 72 mJ/m^2 in a simple Bragg-Williams approximation.[6] and 103 mJ/m^2 in more accurate CVM work.[41] In the present work, the (111) APB energy has been computed by designing a large supercell which contained the APB and comparing its formation energy calculated with the cluster expansion [Eq. (6)] with that of the perfect $L1_2$ phase. We find a (111) APB energy of 85 mJ/m^2 which is of the same order as that obtained in previous theoretical work, and significantly less than the experimental values. It is gratifying that a fully first-principles result agrees about just as well with the experimental data as what can be achieved with fitting. Under compression of 5.4 GPa, the cluster expansion predicts that the (111) APB energy should increase insignificantly to 88 mJ/m^2. That phase diagram work underestimates the APB energy is a surprising result. In the calculated APB energies the effect of relaxation and chemical disorder at the the boundary have been ignored. Both effects reduce the APB energy in actual APB's and thus the calculated values should be greater than the experimental values. A possible explanation might be that the Ising-type parametrization of configurational internal energy is approximate only. When temperature-independent ECI's are obtained from a fit to the experimental phase diagram, highly temperature-dependent contributions from vibrational and electronic excitations are ''mapped'' onto an Ising-like Hamiltonian. Such a procedure must introduce a certain error. In the current work, vibrational and electronic excitations are neglected altogether. Considering that the APB energies are in reasonable agreement with experimental data it appears that these errors are not very large.

As mentioned above, at a hydrostatic pressure of 5.4 GPa Al and Li are predicted to have almost identical atomic volumes in the pure element states, so that at this pressure Al-Li is an alloy without any atomic size difference. At high pressure the deviation from Vegard's rule has the same sign as in the uncompressed alloy, but clearly the contraction upon alloying has become much smaller. The large influence of the state of order on the volume per atom remains for equiatomic bcc-based structures: the lattice parameter of the $B11$ structure is still 4% larger than that of the $B2$ structure. At 5.4 GPa hydrostatic pressure, the ground states on the Li-rich side change: On the fcc lattice the $L1_0$ AlLi structure is replaced by the $K40$ ground state, which is almost degenerate with the $L1_0$ state of order, and at composition $AlLi_3$ a marginally stable DO_{22} ground state emerges. On the bcc lattice, the $B32$ structure remains by far the most stable ordered state, but compression stabilizes the $AlLi_3$ DO_3 phase sufficiently to break the convex hull. Although compression enhances the ordering tendencies at Li-rich compositions, the Al_2Li_3 and Al_4Li_9 phases remain stable with respect to the bcc and fcc superstructures. Therefore, the DO_3 phase, even at high pressure, is still not a stable phase. As one might expect on the basis of a naive dense packing argument, the structural energy difference between fcc and bcc shifts in favor of the fcc structure at this high pressure both for pure Al and pure Li. At pressures over 2 GPa, Mehl[34] has found that bcc Li becomes mechanically unstable because the shear modulus, $C_{11}-C_{12}$, vanishes. In other recent work too,[43] it has been shown that a given element or intermetallic compound may not be mechanically stable in certain crystal structures. Here we will only consider stability with regards to isotropic deformations and short- and long-range ordering. This means that when a phase is found to be stable, it still can be unstable with respect to a degree of freedom not considered here.

B. BCC phase equilibria at nonzero temperature

At finite temperatures, phase equilibria were computed with the CVM. First, the zero-pressure phase diagrams will be discussed. The bcc based phase diagram is shown in Fig. 6(a). It displays, as expected on the basis of the ground state analysis, only one intermetallic phase, the AlLi $B32$ phase,

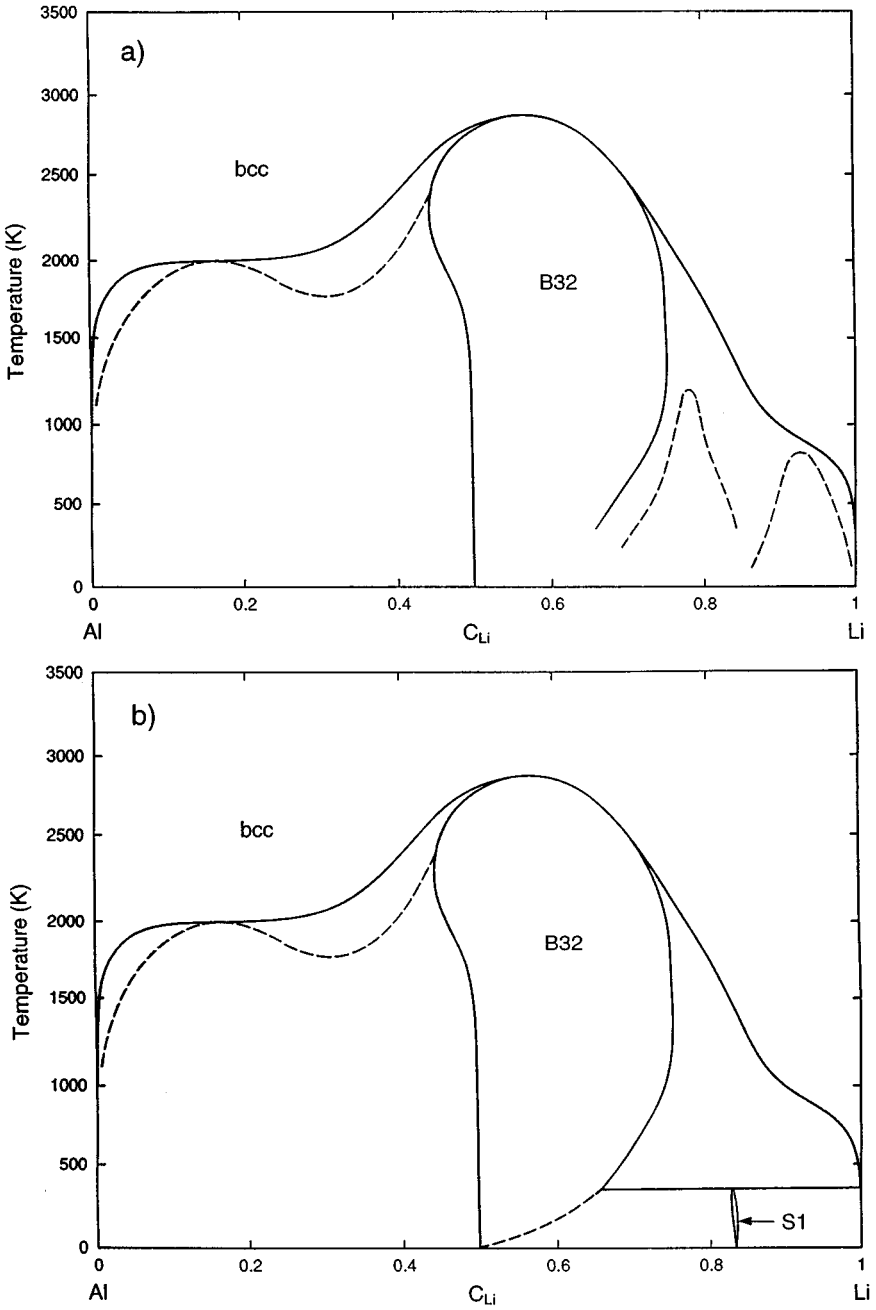

FIG. 6. The bcc-based Al-Li phase diagram at zero pressure, without (a) and with (b) the $S1$ ordered structure. Lines: binodals (solid), $\langle 000 \rangle$ spinodals (dashed).

which remains ordered up to very high temperature. In fact, the $B32$ order-disorder temperature is well above the experimental melting temperature, which means that this phase melts before disordering occurs, as is indeed observed in actual alloys.[3] Another feature of interest is that the $\langle 000 \rangle$ spinodal follows just below the solubility line of the bcc (SS). This implies that bcc SS's are unstable in a large composition and temperature region. Analysis of the eigenvectors of the second derivative matrix of the Gibbs free energy reveals that the instability results from a chemical short-range order effect. The implication is that in oversaturated Al-rich Al-Li alloys one could never form a bcc SS in place of the $B32$ phase. If the $B32$ type of ordering is somehow prevented from taking place, no bcc SS could develop.

The $B32$ single-phase region is skewed towards the Li-rich side. Clearly, in the $B32$ phase Al sites can be filled with Li atoms, but the reverse is energetically too costly. This has been observed in actual alloys. It has been shown that in Li-rich $B32$, Li atoms substitute for Al atoms, whereas in Li-poor alloys Li-site constitutional vacancies occur as the dominant defect.[44–46] A similar effect occurs in the fcc phase diagram with the Al_3Li $L1_2$ phase also. This $L1_2$ phase is predicted to have a significant substitutional solubility for excess Li, but not for Al. In both cases the underlying phenomenon is the same: at the Al-rich side of stoichiometry only very unfavorable structures occur and phase separation tendencies emerge. Li vacancies are more likely to occur than Al vacancies because the vacancy formation energy is approximately proportional to the number of valence electrons per atom.[47,48] The presence of a "buried" miscibility gap (MG) at Al-rich compositions is evidenced by the shape of the $\langle 000 \rangle$ spinodal.

The $\langle 000 \rangle$ spinodals on the Li-rich side display a curious feature: there is a pronounced dip down to zero temperature

TABLE VI. Calculated and measured bulk moduli in GPa. LMTO-ASA (this work) and FLAPW refer to first principles results at 0 K.

Structure	bulk modulus			
	LMTO-ASA	FLAPW (Ref. 34)	FLAPW (Ref. 14)	Experiment
Al fcc	84.4	82.4	82.2	83.3 (Ref. 61)
Al_3Li $L1_2$	69.1	70.0	70.3	66 (Ref. 36)
Li bcc	15.2	15.1	15.2	12.0 (Ref. 62)
Li fcc	14.7	15.0	13.6	

in the vicinity of $c_{Li}=0.85$. This suggests that there could be a stable structure. However, none of the known bcc ground state structures[30] was found to be stable on the bcc lattice at this composition. The correlation functions which minimize the free energy can be found by doing a CVM computation for the disordered phase down to zero temperature because the short-range order in the disordered state, with very few exceptions,[49] mimics the long-range order.[50] Using specially defined correlation functions, it was found that pure Al clusters could only occur for the point and the third *nn* pair. All other cluster correlations had zero probability for pure Al occupancy. Moreover, the zero-temperature correlation functions indicated that for every Al atom there are two third NN's of Al-Al type. The simplest structures that fulfill these conditions consist of mixed Al-Li occupancy (100) planes where each Al atom is surrounded by four Al atoms in the third NN shell and where these mixed (100) are separated by two or more pure Li (100) planes. The highest symmetry layered structures of this type are shown in Fig. 1. The structure labeled "$S1$" was found to be the most stable. Considering that these structures were not found in the ground state analysis with first, second, third, and fifth NN pair interactions[30] indicates that they are stabilized by many-body ECI. The $AlLi_5$ $S1$ phase is stable up to about 300 K as is shown in Fig. 6(b), and the $AlLi_6$ $S2$ and $AlLi_7$ $S3$ phases do not occur. The $S1$ phase is not stable with respect to a mixture of the Al_4Li_9 and Li fcc phases. There also is no high temperature bcc SS from which it is likely to be formed and therefore it is unlikely that this phase will ever be observed. The $S1$ phase should not be confused with the $AlLi_5$ phase in a revision[51] of an earlier assessment.[4] The new version[51] is inconsistent with the accompanying text and with any of its references to previous work, so that it is most likely that an error has been made in the drawing of the phase diagram.[52]

Although in the present calculation (1) more distant ECI's have been taken into account and (2) many more ordered configurations were used for the determination of those ECI's, and (3) a more accurate, larger maximal cluster was used in this phase diagram calculation than in the previously computed first-principles phase diagram (Fig. 6 in Ref. 14) the results are rather similar. The difference is quantitative, the temperature scale in the present calculation is somewhat higher.

Under compression the bcc-based phase diagram changes as follows: (1) a rather stable $AlLi_3$ DO_3 phase emerges, and (2) the $AlLi_5$ $S1$ phase disappears, (3) the order-disorder temperature of the $B32$ phase is increased slightly, (4) and the single-phase region of the $B32$ is expanded (see Fig. 7).

C. fcc phase equilibria at nonzero temperature

The zero-pressure fcc-based phase diagram displays more intermetallic phases. Fig. 8 exhibits a prominent Al_3Li $L1_2$ phase, the $L1_0$, $C2/m$ Al_2Li_4 and $C2/m$ $AlLi_5$ phases, as well as a minor MG at high Li concentrations. It should be remarked that the $L1_0$ and $C2/m$ phases are all unstable above room temperature and hence cannot be observed experimentally. These phases are not stable with respect to the Al_2Li_3 and Al_4Li_9 phases, so that the features associated with the $L1_0$ and $C2/m$ phases are of little practical interest. The Al_3Li $L1_2$ phase, however, is of great interest and some striking experimental features are accurately reproduced: Unlike earlier work[14] the two-phase region between the Al-rich fcc SS and the $L1_2$ phase has almost the correct width. The metastable solubility limit of Li in the Al-rich SS is somewhat overestimated. It is correctly predicted that the $L1_2$ phase should precipitate with near stoichiometric composition, and the corresponding Li solubility in the fcc matrix is predicted to approach zero at low temperatures.[4] Based on experimental observations,[2] and on a phenomenological fit to experimental data,[5] it has been surmised that there should be a MG "buried" at low temperature, in the sense that local phase separation would be observed if the order-disorder fcc equilibrium, itself metastable with respect to the fcc-$B32$ equilibrium, were prevented from occurring. Figure 8 exhibits such a MG which is induced by the short-range order. Figure 8 also shows that the $L1_2$ phase can occur up to about 400 °C, which is in excellent agreement with the highest temperatures of about 350 °C at which metastable $L1_2$ precipitates have been observed in actual Al-Li alloys.[53] The predicted misfit parameter is very small. At temperatures above 100 °C, the lattice parameter of the Al_3Li phase is about 1% smaller than that of the fcc Al-rich SS. The observed misfit is even smaller than the one computed here.[53]

A comparison with the previous first-principles phase diagram (Fig. 5 in Ref. 14) reveals that the current result agrees much better with the experimentally observed fcc-$L1_2$ phase equilibria. Clearly, the more accurate treatment afforded by the larger cluster in the CVM, and the much higher accuracy in the cluster expansion for the configurational energy are required. There has been substantial controversy over whether and for which compositions and temperatures the precipitation of the Al_3Li phase is of a spinodal or of a nucleation and growth type. Here we find that the $\langle 100 \rangle$ ordering spinodal is some 100–150 °C below the fcc binodal, which agrees with previous phase diagram fitting results using the tetrahedron-octahedron CVM,[41] and the less accurate Bragg-Williams (BW) method.[6] However, as the metastable Li solubility limit is somewhat overestimated, the

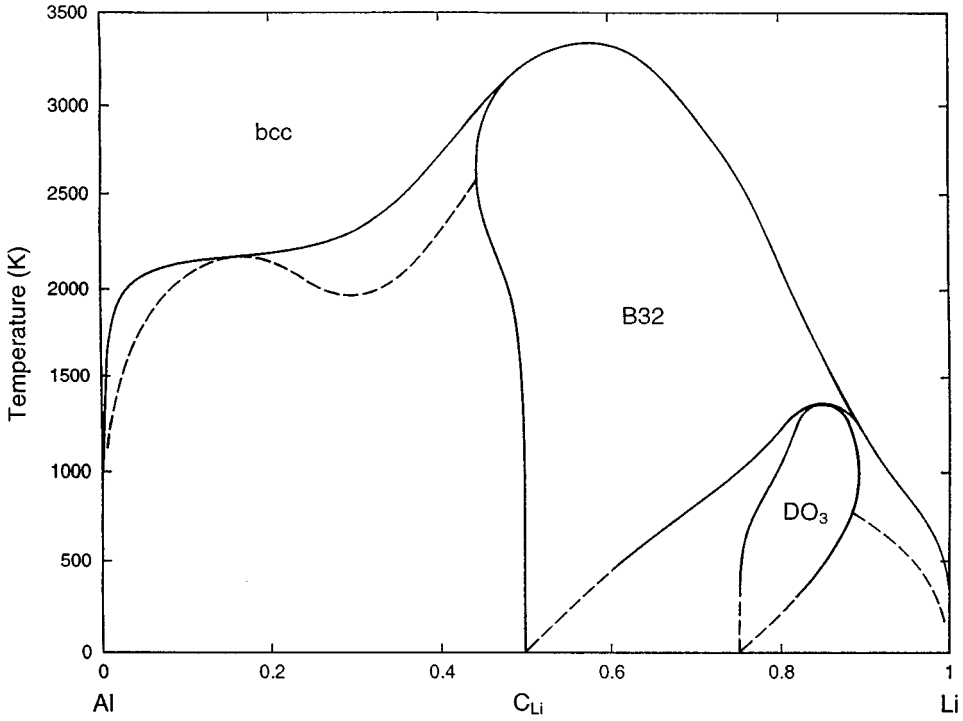

FIG. 7. The bcc-based Al-Li phase diagram at 5.4 GPa pressure, lines as in Fig. 6.

location of the ⟨100⟩ spinodal too, is computed to be at higher Li concentrations than is experimentally observed.[39,54,55]

Concerning previous ''fitted'' metastable $L1_2$ equilibria a comment is in order. In the BW approximation the higher-temperature phase boundaries of the $L1_2$ phase, which are not displayed in Fig. 10 of Ref. 6, behave incorrectly; the calculation gives a second-order transition at 50 at. % (instead of close to 25%) at a temperature of about 1000 K. These features are clearly incorrect and are caused by the use of a ''single-site'' mean field approximation in a frustrated (fcc) system. In contrast, in the work by Sanchez *et al.*[5,41] and in the present calculation the CVM approximation is employed which gives correct topological and quantitative features of the phase diagrams for frustrated systems.

Under compression, as mentioned above, there is a minor change in the ground states at Li-rich compositions. At temperatures well below 50 K, an $AlLi_3$ DO_{22} phase forms (not indicated in Fig. 9). Around equiatomic compositions, pressure enhances the ordering tendencies appreciably, so that the region of fairly strong ordering tendencies is expanded towards more Li-rich compositions. For Al-rich compositions, the changes with compression are rather gradual and minor. The most noticeable is the increase in the ⟨100⟩ spin-

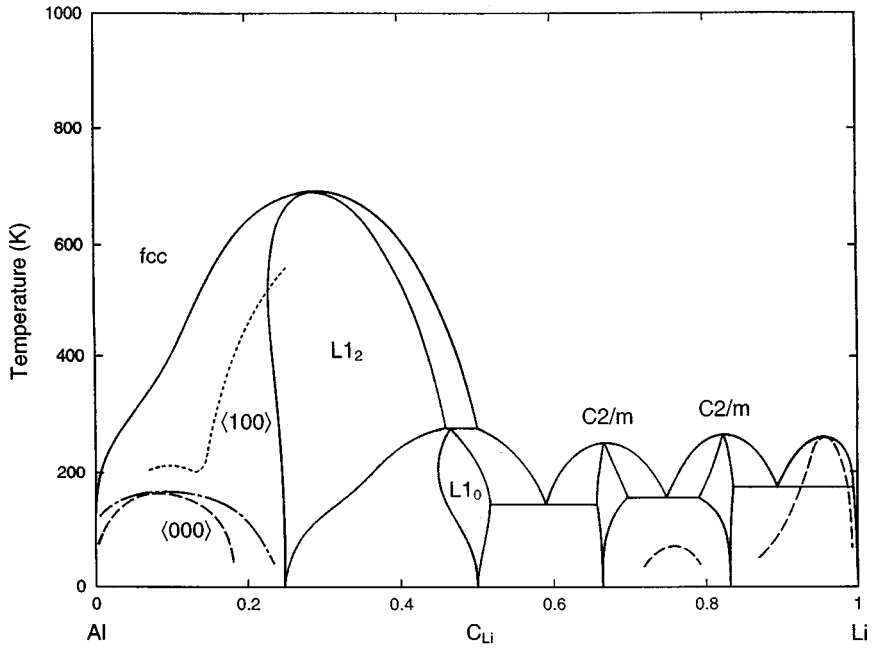

FIG. 8. The fcc-based Al-Li phase diagram at zero pressure. Lines: binodals (solid), ⟨000⟩ spinodals (dashed), metastable MG (chain-dashed), ⟨100⟩ spinodal (dotted).

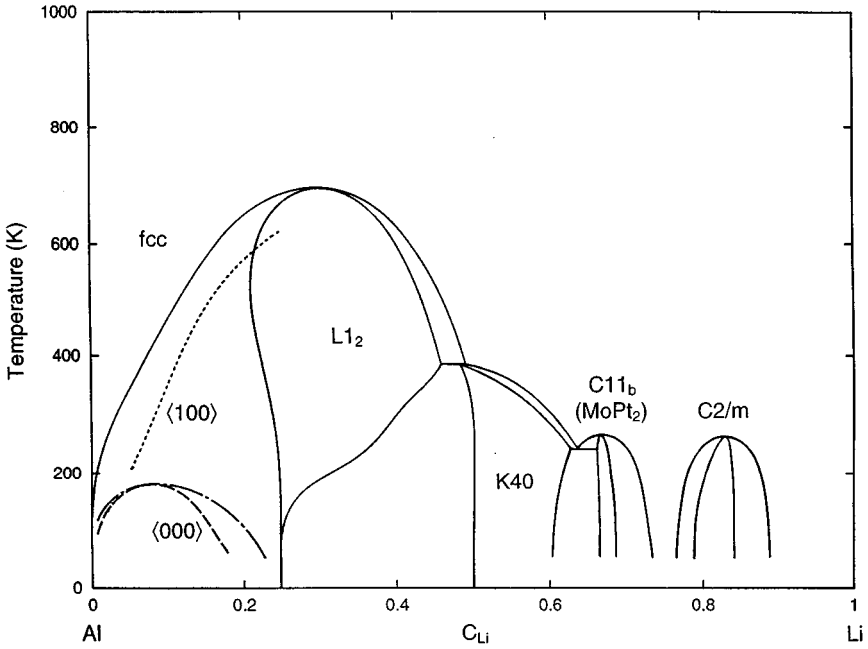

FIG. 9. The fcc-based Al-Li phase diagram at 5.4 GPa pressure, lines as in Fig. 8.

odal temperature, which now is only 50–100 °C below the fcc binodal. This means that under high-pressure nucleation and growth behavior will tend to be replaced by spinodal ordering. Minor effects with pressure are a very slight increases in the order-disorder temperature of the Al_3Li $L1_2$ phase, and in the maximum temperature of the buried MG (see Fig. 9). At 5.4 GPa compression, the solubility limit of Li in the Al-rich fcc matrix in equilibrium with the $L1_2$ phase is only very slightly decreased, which means that at high pressure the composition and temperatures for precipitation remain practically unchanged. Comparison of the equilibrium lattice parameters of the $L1_2$ and fcc SS phases indicates that pressure reduces the misfit parameter to very small values. Hence, under compression the precipitate-matrix interface will remain perfectly coherent.

D. The Al-Li phase diagram

A better comparison with experiment can be made by combining the bcc and fcc phase diagrams and by including the ''interloper'' Al_2Li_3 and Al_4Li_9 phases. At zero pressure, the only stable phases are computed to be Al-rich fcc, AlLi $B32$, and at the Li-rich side both fcc and bcc, see Fig. 10. In addition, the metastable $L1_2$ phase and its two-phase region with the Al-rich fcc SS have been shown. It can be noted that the Li solubility limit in the Al-rich SS and the width of the $B32$ single-phase region are underestimated. Except for those quantitative differences, the agreement with the solid-phase part of the experimental phase diagram is striking. The correct phases are indicated and their composition and temperature ranges are qualitatively correct. The computed Al_3Li $L1_2$ order-disorder temperature is just

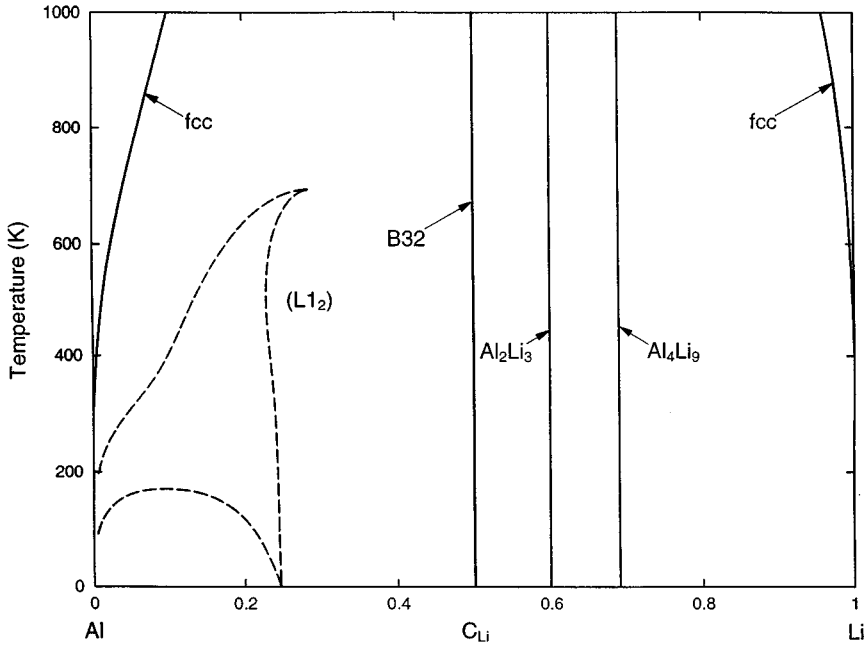

FIG. 10. The complete Al-Li phase diagram at zero pressure. Lines: binodals (solid), metastable fcc-$L1_2$ binodals (dashed).

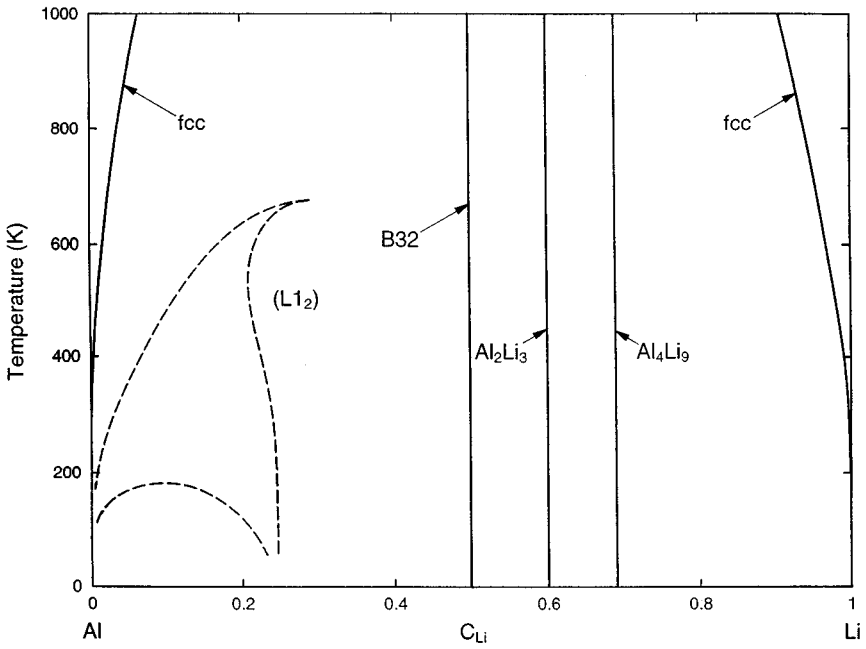

FIG. 11. The complete Al-Li phase diagram at 5.4 GPa pressure, lines as in Fig 10.

above the highest temperature at which $L1_2$ precipitates are observed, and the $L1_2$ fcc two-phase region exhibits a good qualitative agreement with that determined in actual alloys. The low-temperature metastable MG for Al-rich fcc-based alloys, which has been postulated in previous work,[2,5] has been found. Without such a low temperature MG, the $L1_2$-fcc two-phase region tends to be much narrower[14] than is experimentally observed.

About the quantitative shortcomings of the computed phase diagram, we note the following: The too low value for the Li solubility limit in the fcc SS might be due to the neglect of the vibrational degrees of freedom. We expect the free energy of the SS to be lowered more than that of the $B32$ phase because the SS has a lower melting point, and because the stiffness of the $B32$ structure is greater than the average of its constituents.[56] Recently Garbulski and Ceder[57] have shown that, in the harmonic approximation, the ECI at high temperature can be modified considerably when the spring constants between unlike atomic species differ from the geometric mean. The high relative stiffness of the $B32$ phase destabilizes it with respect to less stiff competing phases because those phases can lower their free energies more by vibrations than the $B32$ will. Neglect of vibrational effects is also responsible for the absence of an fcc to bcc transformation at finite temperature in pure Li.

In the bcc phase diagram it was predicted that the $B32$ phase has a significant solubility for Li but not for Al, as was discussed above. However, in the presence of the very stable Al_2Li_3 phase the solubility for Li almost completely disappears. Apparently, our calculations somewhat overestimate the formation energy of the Al_2Li_3 phase. At 5.4 GPa compression the solubility of Li in the Al-rich fcc matrix is reduced by some 35% (see Fig. 11). Indeed, experiments and a simple argument based on experimentally measured parameters[8] indicate that at a given temperature the Li solubility limit should decrease with pressure. At 600 °C the experimentally observed reduction is about 25%.[8]

It has been shown that under compression Al-Li alloys can be prepared with much higher Li concentrations in the fcc SS (Ref. 8) than is possible under ambient pressures. This is due to the great increase in the melting temperature of Al-rich Al-Li alloys under pressure. The large melting point increase in turn is caused by the large expansion of Al-rich alloys upon melting.

Our results indicate that at high pressure the formation energies of the $L1_2$ and $B32$, and other ordered phases (see Table IV), become slightly more negative. That is, compression enhances ordering in this system.

The strong ordering tendencies of $\langle 100 \rangle$ type in Al-rich fcc alloys contradict some results reported with the KKR-ASA-CPA-GPM.[58] In that work the NN EPI is found to be strongly negative, indicative of phase separation. This result must be incorrect because the $L1_2$ phase is (meta)stable, and because several independent local density approximation calculations, including this work, have shown that the $L1_2$ phase is stable with respect to phase separation on the fcc lattice.[14,59,34] Hence the sign of the NN EPI should be positive.

IV. CONCLUSION

The solid-phase portion of the Al-Li composition-temperature phase diagram has been computed from first principles at zero pressure and at 5.4 GPa. Although this calculation does not contain adjustable parameters, the result agrees well with available experimental observations. Specific correct features of the calculation are: (1) Close-packed structures for both pure Al and Li are more stable than bcc at absolute zero of temperature. (2) The lattice stability difference for Li at 0 K between bcc and fcc is small enough to be compensated for by vibrational contributions at higher temperatures in favor of the more ''open'' bcc structure. (3) The $B32$ structure is much more stable than other equiatomic ordered configurations, such as $B2$, $B11$, $L1_0$, and $K40$. (4) The Al_3Li-$L1_2$ phase exists as a metastable ordered state. (5) The calculated congruent order-disorder temperature of the metastable Al_3Li-$L1_2$ phase falls within the wide scatter of its experimental determination. (6) The correct width of the

fcc-Al_3Li $L1_2$ two-phase field. (7) The small negative value of the misfit between the Al-rich SS and the Al_3Li-$L1_2$ phase. (8) The relatively high solubility of Li in fcc Al which increases with temperature and the very small solubility of Al in both fcc and bcc Li. (9) The AlLi phase ($B32$) being so stable that it melts before disordering takes place. (10) The asymmetry in the Al and Li solubility in AlLi $B32$ and Al_3Li $L1_2$. (11) The low-temperature MG in Al-rich alloys, itself metastable with respect to metastable order-disorder fcc phase separation. (12) The decrease of the bulk modulus with increasing Li content. (13) The stability of the Al_2Li_3 and Al_4Li_9 ''interloper'' phases. Clearly, the phase diagram computed in this work is in much better qualitative and quantitative agreement with experiment than the previous *ab initio* result.[14]

Using about 10–20 ordered configurations to obtain a cluster expansion for the configurational internal energy is apparently sufficient to accurately model the configurational aspects of alloying. A remaining shortcoming is that the vibrational degrees of freedom are not considered. As a result, the fcc-bcc transformation in pure Li is not modeled, and the Li solubility in fcc Al-rich SS may be underestimated. Another quantitative shortcoming of the first principles phase diagram is the underestimated width of the $B32$ single-phase region. The computed width is less than 1% at all temperatures below the actual melting point, whereas the assessment gives a maximum width of 8%.[4] This discrepancy may be due to an overestimated formation energy of the Al_2Li_3 phase, or may result from inaccuracies in the assessment. The latter is possible because there is experimental data that suggests a much narrower single-phase region (see Fig. 3 in Ref. 4).

Our calculations indicate that the Al-Li system should not be affected by high hydrostatic compression. Only very minor effects, such as the reduced Li solubility in the Al-rich fcc SS are predicted. The reduction of the Li solubility at 5.4 GPa is about 35%, in reasonable agreement with the experimental estimate of 25%.[8] We also predict that compression should very slightly enhance the solubility of Al in Li.

The (111) APB energy has been computed to be about 85 mJ/m^2. This value lies between the values obtained previously[6,41] by fitting to experimentally determined thermodynamic data, and, just as in previous calculations, it is significantly less than that measured experimentally.[40,39]

Using a new set of correlation functions it has been shown also how one can quite easily deduce an unknown ground state structure. As an example the structures in Fig. 1 were given.

Atomic size mismatch, which in some other alloy systems[10,11] is so important, here hardly plays a role. The 18% difference in volume per atom in pure Al and pure Li at ambient pressures can be eliminated by a hydrostatic compression of 5.4 GPa. However, we find that this pressure hardly alters the phase equilibria at all. On the fcc and bcc lattices we find that eliminating the size mismatch very weakly enhances the ordering tendencies. We conclude that the atomic size difference with reference to the pure elements is not very meaningful in this alloy. More meaningful is a comparison of the partial atomic volumes (defined in Ref. 14). In Al-rich alloys, the Al and Li partial atomic volumes are almost identical (see Fig. 4), and hence these alloys behave as perfectly lattice matched systems.

ACKNOWLEDGMENTS

One of the authors (M.S.) gratefully acknowledges the visiting professorship funded by Hitachi Corporation and the hospitality of The Institute for Materials Research at Tohoku University. The authors thank Dr. M. van Schilfgaarde for a critical reading of the manuscript and for providing LMTO-ASA programs. Portions of the work carried out at Berkeley were supported by the Director, Office of Energy Research, Office of Basic Energy Sciences, Materials Sciences Division of the U.S. Department of Energy under Contract No. DE-AC03-76SF00098.

*Present address: Brookhaven Nat'l. Lab, Department of Physics, Upton, N.Y. 11973.

[1] M.L. Saboungi and C.C. Hsu, Calphad **1**, 237 (1977).
[2] F.W Gayle and J.B. van der Sande, Bull. Alloy Phase Diagrams **5**, 19 (1984).
[3] R. P. Elliott and F.A. Shunk, Bull. Alloy Phase Diagrams **2**, 353 (1981).
[4] A.J. McAlister, Bull. Alloy Phase Diagrams **3**, 177 (1982), and references therein.
[5] C. Sigli and J.M. Sanchez, Acta Metall. **34**, 1021 (1986).
[6] A.G. Khachaturyan, T.F. Lindsey, and J.W. Morris, Jr., Met. Trans. **19A**, 249 (1988).
[7] V.A. Phillips, Acta Met. **9**, 216 (1961).
[8] A. Matsumuro, K. Sakai, and M. Senoo, J. Mater. Sci. **28**, 6567 (1993).
[9] Z.W. Lu, S.-H. Wei, and A. Zunger, Europhys. Lett. **21**, 221 (1993).
[10] C. Amador, W.R.L. Lambrecht, M. van Schilfgaarde, and B. Segall, Phys. Rev. B **47**, 15276 (1993).
[11] D.D. Johnson, J.B. Staunton, and F.J. Pinski, Phys. Rev. B **50**, 1473 (1994).
[12] P.P. Singh, A. Gonis, and P.E.A. Turchi, Phys. Rev. Lett. **71**, 1605 (1993).
[13] H.L. Skriver, *The LMTO Method*, Springer Series in Solid State Sciences, Vol. 41 (Springer, Heidelberg, 1983); O.K. Anderson, O. Jepsen, and D. Glotzel, in *Highlights of Condensed Matter Theory*, Proceedings of the International School of Physics ''Enrico Fermi,'' Course **89**, edited by F. Bassani, F. Fermi, and M.P. Tosi (North-Holland, Amsterdam, 1985), p. 59. (The actual code was graciously provided by Dr. M. van Schilfgaarde.)
[14] M. Sluiter, D. de Fontaine, X.Q. Guo, R. Podloucky, and A.J. Freeman, Phys. Rev. B **42**, 10460 (1990).
[15] M. Asta *et al.*, Phys. Rev. B **46**, 505 (1992).
[16] R. McCormack *et al.*, Phys. Rev. B **48**, 6767 (1993).
[17] C. Wolverton, G. Ceder, D. de Fontaine, and H. Dreysse, Phys. Rev. B **45**, 13105 (1992).
[18] Z.W. Lu, S.H. Wei, and A. Zunger, Phys. Rev. B **44**, 512 (1991).
[19] R. Kikuchi, Phys. Rev. **81**, 988 (1951).
[20] D. de Fontaine, in *Solid State Physics*, edited by H. Ehrenreich, F. Seitz, and D. Turnbull (Academic Press, New York, 1979), Vol. 34, p. 1; D. de Fontaine, in *Solid State Physics*, edited by H. Ehrenreich and D. Turnbull (Academic Press, New York, 1994), Vol. 47, p. 80.
[21] J.M. Sanchez, F. Ducastelle, and D. Gratias, Physica A **128**, 334 (1984).

[22] D.A. Hansen and J.F. Smith, Acta Crystallogr. B **24**, 913 (1968).
[23] J.L.C. Daams, P. Villars, and J.H.N. van Vucht, *Atlas of Crystal Structures for Intermetallic Phases* (ASM International, Materials Park, OH, 1991), p. 830.
[24] K.F. Tebbe, H.G. von Schnering, B. Ruter, and G. Rabanek, Z. Naturforsch. Teil B **28**, 600 (1973).
[25] H.G. Smith, Phys. Rev. Lett. **58**, 1228 (1987).
[26] J.W. Connolly and A.R. Williams, Phys. Rev. B **27**, 5169 (1983).
[27] G.D. Garbulski and G. Ceder, Phys. Rev. B **51**, 67 (1995).
[28] G. Ceder, G.D. Garbulski, and P.D. Tepesch, Phys. Rev. B **51**, 11257 (1995).
[29] T. Mohri, J.M. Sanchez, and D. de Fontaine, Acta Metall. **33**, 1171 (1985).
[30] A. Finel and F. Ducastelle, in *Phase Transformations in Solids*, edited by T. Tsakalakos (North-Holland, Amsterdam, 1984), p. 293.
[31] M.J. Richards and J.W. Cahn, Acta Metall. **19**, 1263 (1971).
[32] S.M.Allen and J.W. Cahn, Scr. Metall. **7**, 1261 (1973).
[33] D.A. Vul and D. de Fontaine, in *Materials Theory and Modelling*, edited by J. Broughton, P. D. Bristowe, and J. M. Newsam, MRS Symposia Proceedings No. 291 (Materials Research Society, Pittsburgh, 1994), p. 401; D. de Fontaine, in *Solid State Physics*, edited by H. Ehrenreich and D. Turnbull (Academic Press, New York, 1994), Vol. 47, p. 84.
[34] M. Mehl, Phys. Rev. B **47**, 2493 (1993).
[35] A. Matsumuro, K. Sakai, and M. Senoo, Jpn. Soc. Mech. Eng. Int. J. A **37**, 59 (1994).
[36] W. Mueller, E. Bubeck, and V. Gerold, in *Proceedings of the 3rd International Conference on Aluminum-Lithium Alloys*, edited by C. Baker, P.J. Gregson, S.J. Harris, and C.J. Peel (TMS-AIME, London, 1986), p. 435.
[37] P.E.A. Turchi, M. Sluiter, F.J. Pinski, D.D. Johnson, D.M. Nicholson, G.M. Stocks, and J.B. Staunton, Phys. Rev. Lett. **67**, 1779 (1991), and references therein.
[38] M. Sluiter, P.E.A. Turchi, F.J. Pinski, and G.M. Stocks, Mater. Sci. Eng. A **152**, 1 (1992).
[39] J. Lendvai and H.J. Gudladt, Z. Metallkd. **84**, 242 (1993).
[40] J.C. Huang and A.J. Ardell, Mater. Sci. Eng. A **104**, 149 (1988).
[41] J.S. Garland and J.M. Sanchez, in *Kinetics of Ordering Transformations in Metals*, edited by H. Chen and V.K. Vasudevan (TMS, Warrendale, PA, 1992), p. 207.
[42] J. Kanamori and Y. Kakehashi, J. Phys. (Paris) Colloq. **38**, C7-274 (1977).
[43] P.J. Craievich, M. Weinert, J.M. Sanchez, and R.E. Watson, Phys. Rev. Lett. **72**, 3076 (1994).
[44] K. Kishio and J.O. Brittain, J. Phys. Chem. Solids **40**, 933 (1979).
[45] T.O. Brun, S. Susman, R. Dejus, B. Granelli, and K. Skold, Solid State Commun. **45**, 721 (1983).
[46] K. Kuriyama, T. Kato, T. Kato, H. Sugai, H. Maeta, and M. Yahagi, Phys. Rev. B **52**, 3020 (1995).
[47] W. Jones and N.H. March, *Theoretical Solid State Physics* (Dover, New York, 1973), Vol. 2, p. 997.
[48] F.R. de Boer, R. Boom, W.C.M. Mattens, A.R. Miedema, and A.K. Niessen, in *Cohesion in Metals, Transition Metal Alloys*, edited by F.R. de Boer and D.G. Pettifor, Cohesion and Strucutre Series Vol. 1 (North-Holland, Amsterdam, 1988), pp. 676 and 692.
[49] R. Caudron, M. Sarfati, M. Barrachin, A. Finel, and F. Solal, Physica B **180-181**, 822 (1992).
[50] M. Sluiter (unpublished).
[51] A.J. McAlister, in *Binary Alloy Phase Diagrams*, edited by T.B. Massalski, 2nd ed. (ASM International, Materials Park, OH, 1990), p. 167.
[52] Other inconsistencies in the drawn phase diagram are the incorrect location along the composition axis of the Al_2Li_3 phase, the absence of the Al_4Li_9 phase, the large solubility of Al in bcc Li, and the peritectic at pure Li. In fact, the Al_2Li_3 phase is drawn at the composition of the Al_4Li_9 phase.
[53] D.B. Williams and J.W. Edington, Met. Sci. **9**, 529 (1975).
[54] B. Noble and A.J. Trowsdale, Scr. Met. **33**, 33 (1995).
[55] T. Sato and A. Kamio, Mater. Trans. Jpn. Inst. Met. **31**, 25 (1990).
[56] B. Fultz *et al.*, Phys. Rev. B **52**, 3280 (1995).
[57] G.D. Garbulski and G. Ceder, Phys. Rev. B **49**, 6327 (1994).
[58] A. Gonis, P.E.A. Turchi, M. Sluiter, F.J. Pinski, and D.D. Johnson, in *Phase Stability and Phase Diagrams of Al-Li Alloys*, edited by G.M. Stocks, D.P. Pope, and A.F. Giamei, MRS Symposia Proceedings No. 186 (Materials Research Society, Pittsburgh, 1990), Figs. 3 and 4, pp. 89–94.
[59] K.I. Masuda-Jindo and K. Terakura, Phys. Rev. B **39**, 7509 (1989).
[60] X.Q. Guo, R. Podloucky, J. Xu, and A.J. Freeman, Phys. Rev. B **41**, 12432 (1990).
[61] L.F. Mondolfo, *Aluminum Alloys: Structure and Properties* (Butterworths, New York, 1979), pp. 82 and 308.
[62] E.A. Brandes, *Smithells Metals Reference Book*, 6th ed. (Butterworths, Boston, 1983).